FIRST PRINCIPLE INVESTIGATION OF ROBUSTNESS SURFACE STATES ON TERNARY MIXED CHALCOGENIDE Bi$_2$Te$_2$S

A. *Shuaibu[1], S.G. Abdu[1], Y.A. Tanko[1] and O.A. Kafayat[2]

[1] Department of Physics, Kaduna State University, P. M. B. 2339, Kaduna, Nigeria.
[2] College of Health Science and Technology, Makarfi, Kaduna, Nigeria

*E-Mail: alhazikara@gmail.com

ABSTRACT

In this paper, we present a theoretical investigation on the electronic structures of bulk ternary mixed chalcogenide Bi$_2$Te$_2$S and its corresponding Bi$_2$Te$_2$S (111) surface thin films based on the first principle within the density-functional theory. The spin-orbit coupling (SOC) included self-consistency. We have found that the effect of SOC significantly changes the electronic properties of bulk Bi$_2$Te$_2$S. For the Bi$_2$Te$_2$S (111) surface thin films, we have adopted the method proposed by Park K. *et al* (2010). Our result shows the presence of robustness states on the electronic structure of Bi$_2$Te$_2$S (111) thin films with the presence of a Dirac Point (DP) below the Fermi level E_F that is completely covered in the bulk bands. This result is in agreement with the Topological Insulator (TI) nature in the binary Bi$_2$Te$_3$.

Keywords: Ternary mixed chalcogenide, Surface State, Density functional theory Structural and electronic properties, and Robust Topological Nature of Material

INTRODUCTION

Binary mixed chalcogenide compounds with the formula X$_2$Te$_3$ (X= Bi, Sb) are the most widely studied members of the mixed chalcogenide family that have traditionally been proven to be an exceptional thermoelectric material (Kanatzidis, 1998). They have been observed as materials that can directly convert waste heat into electricity without any moving measures (Ismail and Ahmed, 2009). For more than half century, these materials have been revealed to have large thermoelectric power (Seebeck coefficients) and recently, have been widely used in thermoelectric refrigeration (Rowe, 1995; Goldsmid and Douglas, 1954). These compounds as well as similar compounds of the same family constitute an interesting class of condensed matter called topological insulators (TI) (Zhang *et al*, 2009). The topological insulators are renowned for the existence of metallic spin-helical surface states, which are robust against the presence of nonmagnetic impurities or disorder (Moore, 2010; Steinberg *et al*, 2010). These surface states have potential technological and industrial applications, such as in spintronics (Vobornik *et al*, 2011; Alam and Ramakrishna 2013), quantum computation (Qi and Zhang, 2010; Yazyev *et al*, 2010; Fleurial *et al*, 1988) and thermoelectric energy conversion (Cava *et al*, 2013). Importantly, these applications require a better fundamental understanding of the atomic and electronic structure of the compounds when interfaced with other materials.

Just recently, researchers have extended the search for a material that possesses this TI nature; not only to binary combinations of these family compounds but also to ternary and even quatnary combinations (Chang *et al*, 2011) In this era, ternary Bi$_2$Te$_2$Se has been theoretically observed (Neupane *et al*, 2012) as well successfully synthesized as a 3D TI material (Chis *et al*, 2012) by means of different experimental techniques. Both theoretical and experimental results have indicated Bi$_2$Te$_2$Se as a good compound in the massive Dirac Fermions investigation.

These results have brought more attention to the other ternary combinations of the family; for example, Sb$_2$Te$_2$Se has been theoretically predicted and its properties within a DFT have been investigated. It was found to be a good material for surface quantum transport explanation (Wang and Johnson 2011). Bi$_2$Te$_2$S, Sb$_2$Te$_2$S and Bi$_2$Se$_2$Te also have been observed and investigated as TI materials by using DFT calculations. But with the recent comparison of the theoretical results that have been published so far, it has clearly been indicated that there are a large percentage of inconsistencies in their electronic properties as well as the TI nature of these ternary compounds. For example, the values of the calculated bulk band gap reported for Bi$_2$Te$_2$S and Bi$_2$Te$_2$Se are in the range of 0.18-1.55 eV (Rusinov, Nechaev and Chulkov, 2013; Schnadt *et al*, 2006). To the best of our knowledge, only a few literatures have reported the investigation on the TI nature of ternary Bi$_2$Te$_2$S (Wang and Johnson 2011; Jain *et al*, 2013). Despite their effort, some of the properties, such as robust topological states in the electronic band structure have still not explained in details.

Within this framework, there is a need for details investigations for the electronic properties as well as the TI nature by applying different approaches both theoretically and experimentally. In line with this need, the objective of the present work is to perform a comprehensive theoretical study of the electronic structures of bulk Bi$_2$Te$_2$S based on the density-functional theory (DFT), and also to investigate the topological nature of ternary Bi$_2$Te$_2$S using a method that completely depended on the DFT results.

MATERIALS AND METHOD

Crystal Structure

Mixed chalcogenide compounds are formed between the group V and VI elements of the periodic table. They are normally observed in a layered structure, with the elements of group VI are usually occupying the outmost and central (third) layer. And, the group V elements occupy the second layer in the primitive rhombohedral cell with the space group of $R\overline{3}m$ (No. 166). For example, the structure of the binary Bi$_2$Te$_3$ has a layer stack as Te[1]-Bi-Te[2]-Bi-Te[1]. The positions of the two group VI elements in the stack are not equal; normally, the interlayer distances are different (Wang and Johnson, 2011). The compounds can also be formed as a hexagonal lattice with a number of atomic layers, which also provides the foundation in the slab model for the surface investigation.

The ternary combinations of these families are commonly formed from the substitution of the central-layer element of the binary ones. For example, the ternary Bi_2Te_2S, and Bi_2Te_2Se are obtained from substituting Te in the central layer of Bi_2Te_3 with S and Se respectively (Wang and Johnson, 2011; Rusinov *et al*, 2013), which normally leads to the establishment of slightly smaller lattice constants. Both the bulk and corresponding (111) surface of the ternary Bi_2Te_2S have been observed before (Wang and Johnson, 2011; Schnadt *et al*, 2006) but still, to avoid reputation of the results, we have used the primitive rhombohedral cell of five atoms for the bulk B_2Te_2S, using the atomic parameter reported in (Ong *et al*, 2013; Alhassan *et al*, 2015). For the surface state and TI nature investigation, a six quintuple-layered slab of (2 × 2) super cells in a hexagonal lattice along the (111) direction with a vacuum of 22 Å was constructed by means of GDIS software (Fleming and Rohl 2005) The primitive rhombohedral cell, the Hexagonal and corresponding BZ structures are reported in our published article (Alhassan *et al*, 2015).

Computational Methods

For an excellent experimental synthesis of materials, details comprehensive theoretical investigations will make excellent contributions for clear understanding of the TI nature of the ternary Bi_2Te_2S.Therefore, we have carried out our investigation for the electronic properties of the bulk Bi_2Te_2S on rhombohedral unit cells with five atoms on $8 \times 8 \times 8$ *k*-point mesh, using a plane wave basis set, within a DFT with generalized gradient approximation (GGA) parameterized by Perdew-Burkew-Enzerhof (PBE) exchange correlation function (Adllan and Dal Corso 2011) as implemented in the Quantum ESPRESSO package (QE) (Giannozzi *et al*, 2009). In our calculation, a norm-conserving scalar relativistic and fully relativistic pseudo potentials have been used. From the two sets of the pseudo potentials, the valence and semi core *d* state electrons of $3s^2 3p^6$ and $3s^2 3p^4 3d$, respectively, were included in the case of the S atom; whilst, for atoms Te and Bi, both for the scalar and fully relativistic pseudo potentials, a valance and a semi core *d* state of $5s^2 5p^4 4d^{10}$ and $6s^2 6p^3 5d^{10}$, respectively, were used. All pseudo potentials were generated from the PSLIBRARY of the plane-wave self-consistent field (PWSCF) pseudo potentials online references (Adllan and Dal Corso 2011). A SOC was considered in all the cases and the kinetic energy cut-off of 60 Ry for expanding the plane wave functions has been used. For the surface Bi_2Te_2S (111) band gap a $12 \times 12 \times 1$ *k*-point mesh on the six quintuple-layered slab of the (2×2) super cells stacked on the hexagonal lattice show in Fig. 6 (a) were used. In each layer, relaxed parameters, by applying Broyden-Fletcher-Goldfarb-Shanno (BFGS) algorithm (Battiti and Masulli 1990), where the forces and energy minimization process are considered during the relaxation, have been used. And a broad convergence test has been performed for all parameters and considered to be achieved with the minimum consecutive iterative steps with an energy difference less than 1 meV/Å (Battiti and Masulli 1990).

RESULTS AND DISCUSSION

Our results, discussion will begin with the band structures of bulk Bi_2Te_2S crystals. The calculated band structures without and with SOC effect for Bi_2Te_2S along the symmetry points in BZ are shown in Fig 1. From the figure, we have observed that when SOC was not taken into consideration Fig. 1 (a), the band structure looks similar as the direct bandgap semiconductor with the approximate bandgap value of 0.260 eV at the Gamma-point. But when SOC was

structure looks similar as the direct bandgap semiconductor with the approximate bandgap value of 0.260 eV at the Gamma-point. But when SOC was present Fig. 1 (b), it led to significant energy changes for both the conduction and valence bands, making a clear change for the compound (say from, the direct gap to indirect gap material). One can clearly see that the minimum conduction band and the maximum valence band both occurred within the X–L direction shown in Fig. 1 (a). One significant point to mention is the reduction of the bulk indirect bandgap value to 0.229 eV that occurred due to the presence of SOC shown in Fig. 1 (b). This implies a clear signal of a strong topological insulator property that was similar to the bulk Bi_2Te_2Se (Wang and Johnson, 2011; Alhassan *et al*, 2015).Our results, discussion will begin with the band structures of bulk Bi_2Te_2S crystals. The calculated band structures without and with SOC effect for Bi_2Te_2S along the symmetry points in BZ are shown in Fig 1. From the figure, we have observed that when SOC was not taken into consideration Fig. 1 (a), the band structure looks similar as the direct bandgap semiconductor with the approximate bandgap value of 0.260 eV at the Gamma-point. But when SOC was present Fig. 1 (b), it led to significant energy changes for both the conduction and valence bands, making a clear change for the compound (say from, the direct gap to indirect gap material). One can clearly see that the minimum conduction band and the maximum valence band both occurred within the X–L direction shown in Fig. 1 (a). One significant point to mention is the reduction of the bulk indirect bandgap value to 0.229 eV that occurred due to the presence of SOC shown in Fig. 1 (b). This implies a clear signal of a strong topological insulator property that was similar to the bulk Bi_2Te_2Se (Wang and Johnson, 2011; Alhassan *et al*, 2015).
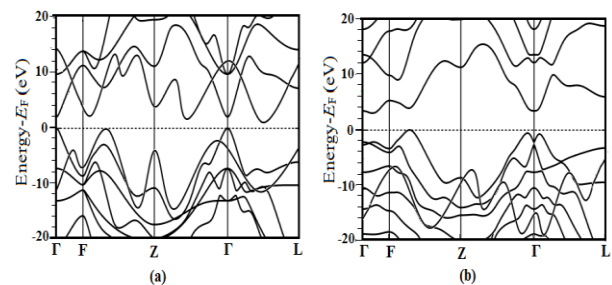

Fig. 1: *The calculated Band structure of bulk Bi_2Te_2S without (a) and with (b) spin–orbit coupling, with the dashed line showing the Fermi level*

We have also obtained the total and projected densities of the states of bulk Bi_2Te_2S crystals shown in Fig. 2 and Fig. 3, respectively. From the result, we have observed that the minimum valence bands were dominated by S 3*s*, Te 4*s* and Bi 5*s* States, which occurred between -9 and 8 eV see Fig. 1 above, while the valence bands were dominated by Bi 6*s* and Te 5*s* states, which occurred between about -9 and -6 eV. The Maximum occupied valence bands were fundamentally dominated by S 3*p*, Te 5*p* and Bi 6*s* states; the 6*p* states of the Bi atoms were also contributing to the valence bands, but the values of the densities of these states were so negligible when compared with that of the S 3*p* and S 5*p* states. The minimum unoccupied conduction bands just above the E_F were dominated by Bi 6*p*. This result indicates the possibility of increases in the hybridization due to the binding of

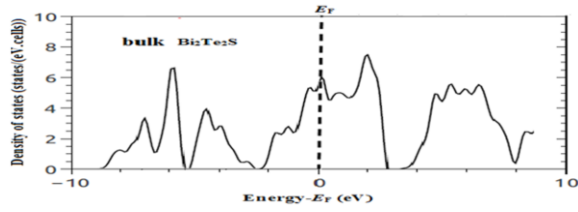the central layer site to two Bi sites which has to be considered during the preparation of ternary Bi₂Te₂S from binary Bi₂Te₃

Fig. 2 The calculated Bulk density of states (DOS) bulk ternary Bi2Te2S. Note that the DOS was calculated without consideration of SOC.

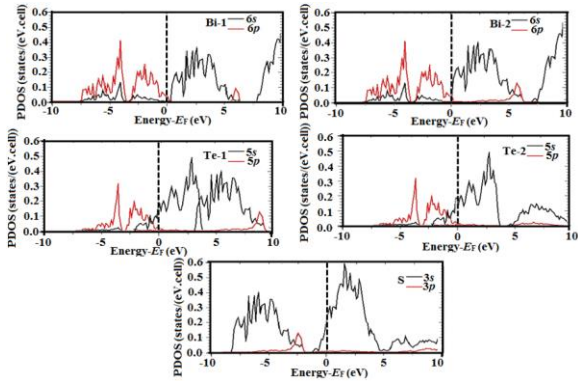*Fig. 3 Projected density of states (PDOS) for both p-like and s-like orbitals of the elements within the bulk ternary Bi₂Te₂S*

For the electronic properties of thin films' investigated, the surface energy, $\gamma_{surface}$, was calculated using the expression (Perkins and DePristo, 1993).

$$\gamma_{sufce} = \frac{1}{A_{sufuce}}\left(E_{slab}^{total} - n_{sufuce}E_{bulk}^{total}\right), \qquad (1)$$

where $E_{slab}^{total}, E_{bulk}^{total}$ represent the total energies of the slab and bulk system, respectively. $n_{surface}$ is the number of the atom in the slab, and $A_{surface}$ is the total surface area of the slab. In each case, we have found 1-6QLs to be stable. The STM calculation was based on the Tersoff-Hamann-approximation (Tersoff and Hamann, 1985) as implemented in the XCrySDen package (Kokalj, 1999). Normally, the calculation is based on the tunneling current $I(r)$ which is given by the expression (Tersoff and Hamann, 1985).

$$I(r) \propto \sum_{E_m > E_F - eV_{biase}}^{E_m < E_F} \left|\psi(r, E_m)\right|^2 = m(r, V_{bias}), \qquad (2)$$

where E_F, E_m are the Fermi energy and energy of state $\psi(r)$, respectively, and V_{bias} is the applied voltage at a specific position r.

Then, we obtained the electronic band structures of the Bi₂Te₂S thin films along the three time reversal symmetry points shows in Fig. 4 (b) by varying the slab thickness from the first QL to six QLs. We have adopted the method reported in (Park *et al*, 2010; Dai *et al*, 2011). The method is only relies on the DFT calculation result quite than using a model Hamiltonian approach, in to precisely classify the topological surface states from the slab band structure of materials with QL structures. In Fig. 5, the pure surface states or bands are indicated with dark red circle, and the corresponding, either bulk-like or surface resonant; states are represented with uncolored lines.
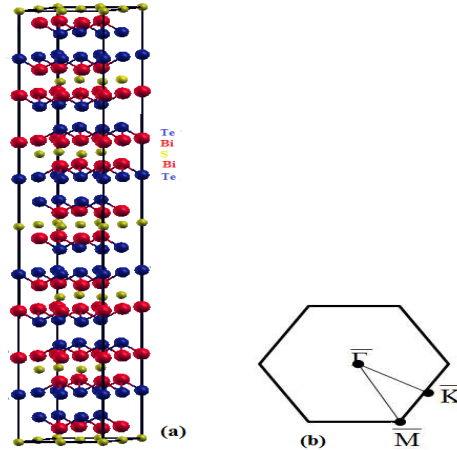

Fig. 4 Schematic diagrams of (a) Bi₂Te₂S thin film structures obtained by stacking 4QLs along the z-direction. (b) Two-dimensional Brillouin zone of the (111) surface within a three time-reversal invariant points

The details of the algorithm can be found in (Park *et al*, 2010), which described that those exact topological surface states from the slab band structure of materials with QL structures can be recognized within a DFT calculation alone. Since normally the obtained surface band structures of the slab model of the surfaces are covered by a bulky band projection partially, it is essential to differentiate between the surface bands from the calculated results. Therefore, for the purpose of comparison, we adopted similar criteria of the critical percentages as described in (Dai *et al*, 2011), the criteria have been established in such a way that the critical percentage of the wave function was projected either on the top or the bottom of the two atomic layers in a given energy band. Thus, for the first QL and second QL, we have used the specified critical percentages of 40% and 35%, respectively; whilst for third, fourth, fifth and sixth QLs, we have used 55%, 60%, 40% and 40%, respectively.

Then, based on the thickness dependence described above, we observed the following. In the first QL (Fig. 5 (i)) of the Bi₂Te₂S film, a closely parabolic band exceeding the E_F has occurred, showing an approximate surface indirect gap ($E_{indirect}$) of about 0.2881eV at the gamma point, and a larger surface gap with an approximate value of 0.4113 at $\overline{\Gamma}$ - reversal symmetry point. Here, there was no surface state that crossed the E_F between the time-reversal-invariant momenta of the QL. For the second QL (Fig. 5 (ii)), a shift in the topmost of the V-shaped band going close to the E_F was observed; while the U-shaped band appeared

below the E_F, leading to the disappearance of the indirect band gap. Also, at the bottom of the V-shaped band, the surface states disappeared, which came from the U-shaped band intersecting the E_F at a point along $\overline{\Gamma} - \overline{M}$ only. This result was not similar to the case of both the binary Bi_2Te_3 reported in (Park *et al*, 2010), and the ternary Bi_2Te_2Se reported in (Dai *et al*, 2011).Where in both cases, the U-shaped band intersected the E_F at two different points crossing the surface state within the second QL film to be topologically insignificant (Park *et al*, 2010; Dai *et al*, 2011).
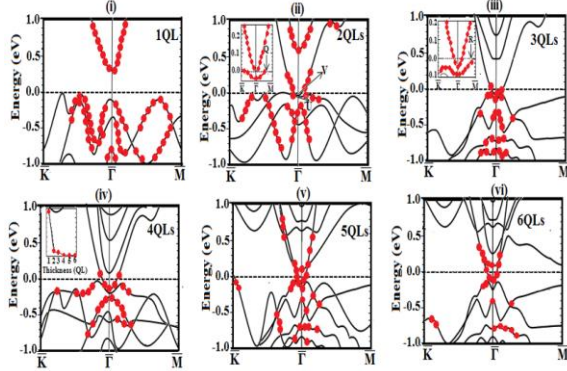

Fig. 5 *The calculated Band structures of Bi₂Te₂S (111) thin films with the thickness range from 1 QL to 6 QLs along the* $\overline{K} - \overline{\Gamma} - \overline{M}$ *direction. The insets in (ii), (iii) and (iv) indicate the zoom-in of the 2 QL, 3 QL and 5 QL band structures near the Fermi level, respectively*

In the third QL film, as indicated in Fig. 6 (iii), it is clearly shown that there were opposite states in the case of both the first and second QL films; in this case, the E_F by the *V*-shaped band shifted down within the third QL film by about 0.016 eV and crossed the E_F along one direction only (say $\overline{\Gamma} - \overline{M}$ directions). Moreover, the U-shaped band along the $\overline{\Gamma} - \overline{K}$ direction occurred under the E_F, with the gap value of less than that of the second QL film. This was similar to the case of Bi_2Te_2Se (Dai *et al*, 2011). For the 4QLs, 5QLs and 6QLs, we have observed a similar surface band very close to the Dirac-like dispersion obtained from the semi-finite film measurement (Dai *et al*, 2011).

Finally, in Table 1, we have shown how the gaps within the whole QLs of the Bi₂Te₂S thin films decreased with increases in thickness. We may have insisted that the indirect gap will disappear when the film becomes thick enough which is in agreement with the results in (Park *et al*, 2010; Dai *et al*, 2011).

Table 1. The energy gap E_{gap} *(e V) at* $\overline{\Gamma}$ *, the number of crossings,* N_c *,of the surface states across the Fermi level,* E_F *, and the indirect energy gap,* $E_{indirect}$ *(e V), as a function of the slab thickness (nm), respectively.*

No of QLs	Thickness	E_{gap}	N_c	E_{indtr}
1	1.1123	0.4113	0	0.2881
2	2.3334	0.1213	1	No gap
3	3.2113	0.0351	1	No gap
4	4.3132	0.0065	1	No gap

We have also observed that, when SOC was taken into consideration, there is no surface band crossing the E_F in case of

all thin films. Also, in Table 2, we have listed the values of the wave function projections onto each QL slab at different specific *k*-points.

Table 2. *Wavefuctions projections on each QL of the 5 QL slabs at the several specific kₖ-points of the V-shaped (U-shaped) band*

	$\overline{\Gamma}_U$	$\overline{\Gamma}_V$	D_U	D_V	E_U	E_V
$k_\parallel \left(2\pi/a\right)$	0.00	0.00	0.016	0.016	0.034	0.034
Uppermost	0.554	0.499	0.611	0.512	0.320	0.231
Upper-1	0.051	0.048	0.062	0.055	0.011	0.002
Middle	0.015	0.006	0.008	0.004	0.006	0.113
Bottommost+1	0.001	0.023	0.000	0.031	0.066	0.215
Bottom+1	0.087	0.002	0.007	0.213	0.211	0.111
Bottommost	0.019	0.034	0.000	0.000	0.001	0.013
Presence of SS?	YES	YES	YES	YES	NO	YES

To observe the surface state more precisely, we have explained the decay length of the surface state in 5QLs, as an example. We have plotted the percentage of the wave function projected onto the top QL of the 5 QL slab shown in Fig.6 (a).
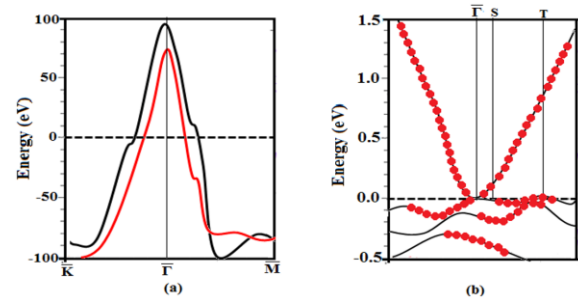

Fig. 6 (a) shows the plot of the percentage of the wavefuctions projected onto the top QL of the 5 QL slab, the V-shaped band is represented with a red line whilst the U-shaped band has the black line. Both the curves indicate a smooth drop in percentages for the higher $k_{//}$ *point. 6 (b) shows the values of the wavefuctions projections onto each QL of the 5 QL slab for both V-shaped and U-shaped bands at different precise k-points*

The *V*-shaped band is represented with a red line while the *U*-shaped band is represented by the red line. Both the curves indicate a smooth drop in percentages for the higher $k_{//}$ point. In this case, we have observed the presence of two surface bands; one was close to the Fermi level and the other closer to the $\overline{\Gamma}$ — point. The behavior of the surface states which intersected the Fermi level had a *V*-shaped band nature and crossed only in the direction of $\overline{\Gamma} - \overline{M}$, while for the bulk state at the Fermi level, we may say that it was from the *U*-shaped band. We have listed the values of the wave function projections onto each QL of the 5 QL slab for both *V*-shaped and *U*-shaped bands at different precise *k*-points in Table 2 (plotted in Fig. 6 (b)). We have observed a rapid decay of the wave function projection at the second QL, which indicates that the dispersion length of the wave function of the surface states was of the order of about 1.8 nm. This was 0.2 less than the observed value obtained in the case of Bi₂Te₂Se (Park *et al*, 2010). From the result, the surface state was observed to be predominantly localized in the topmost QL, while almost completely restrained in the second QL, which obeys the

projected distribution that is shown in Table 2. Also, these types of states were mostly formed by the *pz* orbital of the Bi, Te and S atoms, which reveals the bonding types inside the QL of the bulk Bi_2Te_2S.

Conclusion

In summary, we have presented a comprehensive investigation of the electronic structures of the bulk Bi_2Te_2S and its corresponding Bi_2Te_2S (111) thin films of one to six quintuple layers using first-principle calculations, within DFT as implemented in QE; the effect of SOC was included in our calculations. The topological nature of the surface states in the Bi_2Te_2S (111) thin film has also been investigated by means of a method introduced by Park et al. Our result shows that the bulk Bi_2Te_2S is a topological insulator with similar properties of both the Bi_2Te_3 and Bi_2Te_2Se. Also for the surface investigations, we have emphasized that this method, which is specially based on DFT, gives a precise IT nature of such materials. Also, by observing a surface state on a compound, one can estimate the dispersion depth of the surface states by using the projection on the wave function of each QL of the slab. Our results have also indicated the clear effect of SOC in determining the electronic properties of the bulk Bi_2Te_2S and the presence of a finite gap for the Bi_2Te_2S (111) thin films because of the interaction between the top and bottom surface states. For the Bi_2Te_2S (111) thin films, a significant robust nature of the electronic structure has been observed from the third or more QLs which led to the intersection of Fermi energy once on the Dirac-like surface band at a point (say $\overline{\Gamma} - \overline{M}$ direction). This result has made us emphasize that the Bi_2Te_2S is a TI with a significant topological nature that should lead to a large bulk resistivity required to obtain a feasible electronic device, which is still expected to have experimental proof.

Acknowledgments

REFERENCES

Adllan, A. A., & Dal Corso, A. (2011). Ultrasoft pseudopotentials and projector augmented-wave data sets: application to diatomic molecules. *Journal of Physics: Condensed Matter*, *23*(42), 425501.

Alam, H., & Ramakrishna, S. (2013). A review on the enhancement of figure of merit from bulk to nano-thermoelectric materials. *Nano Energy*, *2*(2), 190-212.

Alhassan, S., Rahman, M., Zainuddin, H., Talib, Z. A., Muhida, R., & Setiyanto, H. (2015). Quasiparticle band structure study of ternary mixed chalcogenide Bi2Te2S as topological insulator. *Chalcogenide Letters*, *12*(2), 85-90.

Battiti, R., & Masulli, F. (1990). BFGS optimization for faster and automated supervised learning. In *International neural network conference* (pp. 757-760). Springer Netherlands.

Cava, R. J., Ji, H., Fuccillo, M. K., Gibson, Q. D., & Hor, Y. S. (2013). Crystal structure and chemistry of topological insulators. *Journal of Materials Chemistry C*, *1*(19), 3176-3189.

Chang, J., Register, L. F., Banerjee, S. K., & Sahu, B. (2011). Density functional study of ternary topological insulator thin films. *Physical Review B*, *83*(23), 235108.

Chis, V., Sklyadneva, I. Y., Kokh, K. A., Volodin, V. A., Tereshchenko, O. E., & Chulkov, E. V. (2012). Vibrations in binary and ternary topological insulators: First-principles calculations and Raman spectroscopy measurements. *Physical Review B*, *86*(17), 174304.

Dai, X. Q., Zhao, B., Zhao, J. H., Li, Y. H., Tang, Y. N., & Li, N. (2011). Robust surface state of intrinsic topological insulator Bi2Te2Se thin films: a first-principles study. *Journal of physics: Condensed matter*, *24*(3), 035502.

Fleming, S., & Rohl, A. (2005). GDIS: a visualization program for molecular and periodic systems. *Zeitschrift für Kristallographie-Crystalline Materials*, *220*(5/6), 580-584.

Fleurial, J. P., Gailliard, L., Triboulet, R., Scherrer, H., & Scherrer, S. (1988). Thermal properties of high quality single crystals of bismuth telluride—Part I: Experimental characterization. *Journal of Physics and Chemistry of Solids*, *49*(10), 1237-1247.

Giannozzi, P., Baroni, S., Bonini, N., Calandra, M., Car, R., Cavazzoni, C., ... & Dal Corso, A. (2009). QUANTUM ESPRESSO: a modular and open-source software project for quantum simulations of materials. *Journal of physics: Condensed matter*, *21*(39), 395502.

Goldsmid, H. J., & Douglas, R. W. (1954). The use of semiconductors in thermoelectric refrigeration. *British Journal of Applied Physics*, *5*(11), 386.

Ismail, B. I., & Ahmed, W. H. (2009). Thermoelectric power generation using waste-heat energy as an alternative green technology. *Recent Patents on Electrical & Electronic Engineering (Formerly Recent Patents on Electrical Engineering)*, *2*(1), 27-39.

Jain, A., Ong, S. P., Hautier, G., Chen, W., Richards, W. D., Dacek, S., ... & Persson, K. A. (2013). Commentary: The Materials Project: A materials genome approach to accelerating materials innovation. *Apl Materials*, *1*(1), 011002.

Kanatzidis, M. G. (1998). Semicond. Semimetals 69, 51 2000; D.-Y. Chung, L. Iordanidis, K.-S. Choi, and MG Kanatzidis. *Bull. Korean Chem. Soc*, *19*, 1283.

Kokalj, A. (1999). XCrySDen—a new program for displaying crystalline structures and electron densities. *Journal of Molecular Graphics and Modelling*, *17*(3), 176-179.

Miyamoto, K., Kimura, A., Okuda, T., Miyahara, H., Kuroda, K., Namatame, H., ... & Kokh, K. A. (2012). Topological surface states with persistent high spin polarization across the Dirac point in Bi 2 Te 2 Se and Bi 2 Se 2 Te. *Physical review letters*, *109*(16), 166802.

Moore, J. E. (2010). The birth of topological insulators. *Nature*, *464*(7286), 194-198.

Neupane, M., Xu, S. Y., Wray, L. A., Petersen, A., Shankar, R., Alidoust, N., ... & Hor, Y. S. (2012). Topological surface states and Dirac point tuning in ternary topological insulators. *Physical Review B*, *85*(23), 235406.

Ong, S. P., Richards, W. D., Jain, A., Hautier, G., Kocher, M., Cholia, S., ... & Ceder, G. (2013). Python Materials Genomics (pymatgen): A robust, open-source python library for materials analysis. *Computational Materials Science*, *68*, 314-319.

Park, K., Heremans, J. J., Scarola, V. W., & Minic, D. (2010). Robustness of topologically protected surface states in layering of Bi 2 Te 3 thin films. *Physical review letters*, *105*(18), 186801.

Perkins, L. S., & DePristo, A. E. (1993). Self-diffusion mechanisms for adatoms on fcc (100) surfaces. *Surface science*, *294*(1), 67-77.

Qi, X. L., & Zhang, S. C. (2010). The quantum spin Hall effect and topological insulators. *Physics Today*, *63*(1), 33-38.

Rowe, D. M. (Ed.). (1995). *CRC handbook of thermoelectrics*. CRC press.

Rusinov, I. P., Nechaev, I. A., & Chulkov, E. V. (2013). Many-body effects on the width of the band gap in Bi2Te2X (X= Te, Se, S) topological insulators. *JETP letters*, *98*(7), 397-402.

Saeed, Y. (2014). *Tuning the Transport Properties of Layered Materials for Thermoelectric Applications using First-Principles Calculations* (Doctoral dissertation, King Abdullah University of Science and Technology).

Schnadt, J., Michaelides, A., Knudsen, J., Vang, R. T., Reuter, K., Lægsgaard, E., ... & Besenbacher, F. (2006). Revisiting the structure of the p (4× 4) surface oxide on Ag (111). *Physical review letters*, *96*(14), 146101.

Steinberg, H., Gardner, D. R., Lee, Y. S., & Jarillo-Herrero, P. (2010). Surface state transport and ambipolar electric field effect in Bi2Se3 nanodevices. *Nano letters*, *10*(12), 5032-5036.

Tersoff, J., & Hamann, D. R. (1985). Theory of the scanning tunneling microscope. In *Scanning Tunneling Microscopy* (pp. 59-67). Springer Netherlands.

Vobornik, I., Manju, U., Fujii, J., Borgatti, F., Torelli, P., Krizmancic, D., & Panaccione, G. (2011). Magnetic proximity effect as a pathway to spintronics applications of topological insulators. *Nano letters*, *11*(10), 4079-4082.

Wang, L. L., & Johnson, D. D. (2011). Ternary tetradymite compounds as topological insulators. *Physical Review B*, *83*(24), 241309.

Yazyev, O. V., Moore, J. E., & Louie, S. G. (2010). Spin polarization and transport of surface states in the topological insulators Bi 2 Se 3 and Bi 2 Te 3 from first principles. *Physical review letters*, *105*(26), 266806.

Zhang, H., Liu, C. X., Qi, X. L., Dai, X., Fang, Z., & Zhang, S. C. (2009). Topological insulators in Bi2Se3, Bi2Te3 and Sb2Te3 with a single Dirac cone on the surface. *Nature physics*, *5*(6), 438-442.